

# Onset of plastic relaxation in the growth of Ge on Si(001) at low temperatures: Atomic-scale microscopy and dislocation modeling

Anna Marzegalli,<sup>\*</sup> Matteo Brunetto, Marco Salvalaglio, and Francesco Montalenti

*Department of Materials Science, Università degli Studi di Milano Bicocca, via Cozzi 53, I-2012 Milano, Italy*

Giuseppe Nicotra, Mario Scuderi, and Corrado Spinella

*CNR-IMM, Strada VIII, 5, 95121 Catania, Italy*

Monica De Seta and Giovanni Capellini

*Dipartimento di Scienze, Università degli Studi Roma Tre, Viale Marconi 446, I-00146 Roma, Italy*

(Received 27 June 2013; revised manuscript received 26 September 2013; published 18 October 2013)

We present a synergic experimental and theoretical investigation of the plastic relaxation onset in low-temperature Ge growth on Si(001). High-resolution transmission electron microscopy reveals that misfit is released by pairs of coupled  $60^\circ$  dislocations. Atomic resolution proved to be key in distinguishing pairs from single  $90^\circ$  dislocations because of the revealed small intrapair dislocation distance (even less than 1 nm). By exploiting dislocation theory and molecular dynamics simulations, we demonstrate that the observed pairing naturally occurs as a result of the mutual interactions between the two dislocations. In particular, analytical models show that the stress field arising in a thin film when a dislocation segment lies at the interface with the substrate determines the most favored nucleation site for a new (complementary) dislocation that leads, after migration, to the coupling with the first in a stable position. At the growth temperature, further motion or recombination due to atomic scale effects is excluded by classical molecular dynamics simulations. A clear picture of the early stages in the strain relaxation emerges, gliding out of the interface and/or short-range climbing (as typically produced by annealing or higher temperature steps but not taking place under the present growth conditions) being required to transform pairs into edge dislocations. The present results also offer answers to the long-asked puzzling question about the mechanism originating  $90^\circ$  dislocation in high-mismatch Ge/Si systems.

DOI: [10.1103/PhysRevB.88.165418](https://doi.org/10.1103/PhysRevB.88.165418)

PACS number(s): 61.72.Bb, 61.72.uf, 68.37.Og

## I. INTRODUCTION

Ge deposition on Si(001) naturally leads to three-dimensional growth of islands (Stranski-Krastanow mode), allowing for a partial relaxation of the misfit deformation.<sup>1</sup> However, when out-of-equilibrium growth conditions are met, as is the case of low-temperature (LT;  $200^\circ\text{C}$ – $400^\circ\text{C}$ ), high-rate (up to a few nanometers per second), or both conditions,<sup>2–4</sup> continuous films can be realized and strain release occurs via plastic relaxation, i.e., via dislocation nucleation. Due to the high strain value associated with the lattice mismatch of 4.2% existing between Si and Ge, dislocations are formed when only few monolayers are deposited.<sup>5</sup> As a consequence, the evolution of Ge layers during the growth at LT is unavoidably related to dislocation nucleation, gliding, and interactions from the early stages.

Although the kinetically limited LT Ge/Si growth dynamics is of paramount technological interest, being the cornerstone of Ge monolithic integration into the silicon photonic platform,<sup>6</sup> a comprehensive understanding of the mechanisms governing from the beginning the plastic strain relaxation is still lacking. Most studies have focused on growth processes comprising postgrowth annealing steps, the use of complex higher temperature (HT) profiles (growth), or both (see e.g., Refs. 3 and 7–9). However, such additional steps induce a peculiar defect evolution, hiding the processes underlying the onset of plasticity, which is the subject of this paper. For this reason, we focused on very thin Ge layers grown entirely at LT. We show that the experimental results can be interpreted

using theoretical modeling relying on either a continuum approach or atomistic simulations, providing a clear scenario and suggesting the further evolution induced by a temperature increase.

In low to moderate Ge content SiGe/Si(001) epitaxial heterostructures, plastic relaxation occurs mainly through the nucleation of dislocation loops (Burgers vectors  $\mathbf{b} = a/2\langle 011 \rangle$ ,  $a$  being the epi-layer lattice parameter) gliding in  $\{111\}$  planes and progressively releasing the epi-layer lattice compression by increasing the loop radius and creating a  $60^\circ$  misfit dislocation segment at the heterointerface, bounded by threading arms reaching the surface. For Ge content higher than 40%, a change in the dislocation character has been reported.<sup>10</sup> Burgers vector analyses ( $\mathbf{g}\cdot\mathbf{b}$  technique) evidenced the presence of edge dislocations at the interface, with their density increasing with a further rise in Ge content and becoming dominant in pure Ge depositions.<sup>10,11</sup> Edge misfit dislocations (often called Lomer dislocations) are characterized by Burgers vectors  $\mathbf{b} = \pm a/2[1-10]$  or  $\mathbf{b} = \pm a/2[110]$  lying in the interface plane. Therefore, they release twice the misfit strain with respect to  $60^\circ$  dislocation segments. However, they cannot be directly nucleated as a loop, because in a perfect diamond lattice, gliding on (100) planes is hindered. Several mechanisms have been proposed to explain the presence and the abundance of edge dislocations in high-misfit SiGe systems.<sup>12–15</sup> One of the most credited hypotheses concerns an induced nucleation mechanism promoting the nucleation and junction of two  $60^\circ$  dislocations, usually called complementary dislocations, characterized by having Burgers vectors giving

rise to Lomer dislocation if joined (e.g.,  $\mathbf{b}_1 = a/2[10\bar{1}]$  and  $\mathbf{b}_2 = a/2[0\bar{1}1]$ , yielding  $\mathbf{b}_1 + \mathbf{b}_2 = \mathbf{b}_3 = a/2[1\bar{1}0]$ ).<sup>10</sup> In particular, it has been suggested that the stress field of a first dislocation already existing at the interface induces the nucleation of a complementary  $60^\circ$  dislocation that has as a glide plane the mirrorlike symmetric glide plane of the first, intersecting it exactly at the interface (ML plane in the following). The new dislocation glides and reaches the one at the interface forming a Lomer segment.<sup>10,16</sup>

Here, we show, through high-resolution electron microscopy (HREM), dislocation theory,<sup>17</sup> and molecular dynamics (MD) simulations, that in few nanometers of LT Ge deposition on Si(001) by chemical vapor deposition (CVD), an induced nucleation mechanism is leading the plastic relaxation but gives rise to closely spaced, paired  $60^\circ$  dislocations, with Lomer formation playing a negligible role. The presence of  $60^\circ$ – $60^\circ$  pairs has been already reported for different growth conditions, in different heteroepitaxial systems, or both,<sup>9,18–20</sup> but never as being dominant over actual  $90^\circ$  dislocations. We show that dominance of pairing vs Lomer formation should be expected based on dislocation theory,<sup>17</sup> in the absence of climbing mechanisms, as the low growth temperature guarantees. We investigate the issue further by a dedicated set of classical MD simulations. Again, we obtain a strong indication that the experimentally observed, closely spaced  $60^\circ$ – $60^\circ$  dislocation pairs (with distinguishable cores) represent a natural configuration for the present system. Because of the small distance between the cores (even less than 1 nm), pairs can be distinguished from an unique edge dislocation segment only if atomic-scale-resolved analysis is carried out<sup>9,21–23</sup> (HREM imaging in this paper). Further evolution, e.g., by a HT growth step or by annealing, is also here discussed.

The results are presented as follows. In the second section, we present the detailed HREM dislocation analysis and the relative findings, along with the sample preparation and growth technique. In the third section, we outline the model developed in the framework of dislocation theory and the results obtain concerning complementary dislocation nucleation and evolution. The fourth section is dedicated to the MD simulations and the relative results on dislocation migration. We summarize the emerging picture of plastic relaxation onset in the last section.

## II. EXPERIMENTAL DETAILS AND HREM RESULTS

Ge layers that are 3 nm thick have been grown on Si(001) substrates by ultrahigh vacuum (UHV) CVD from ultrapure germane, without carrier gas. After a preliminary ultrasonic bath in isopropyl alcohol, the Si(001) substrates sample underwent in situ thermal annealing at  $1100^\circ\text{C}$  in  $\text{H}_2$  atmosphere. In order to ensure a high-quality heterointerface, prior to Ge deposition, a 500-nm-thick silicon buffer layer was deposited using silane UHV-CVD at a deposition temperature of  $800^\circ\text{C}$ . The Ge deposition process pressure was  $1 \times 10^{-3}$  torr, while the CVD reactor base pressure was in the low  $10^{-10}$  torr range, thus allowing deposited materials of high purity. The growth temperature was carefully measured by infrared pyrometer to be  $335 \pm 5^\circ\text{C}$ , and the resulting growth rate was measured to be 0.2 nm/min using transmission electron microscopy (TEM).

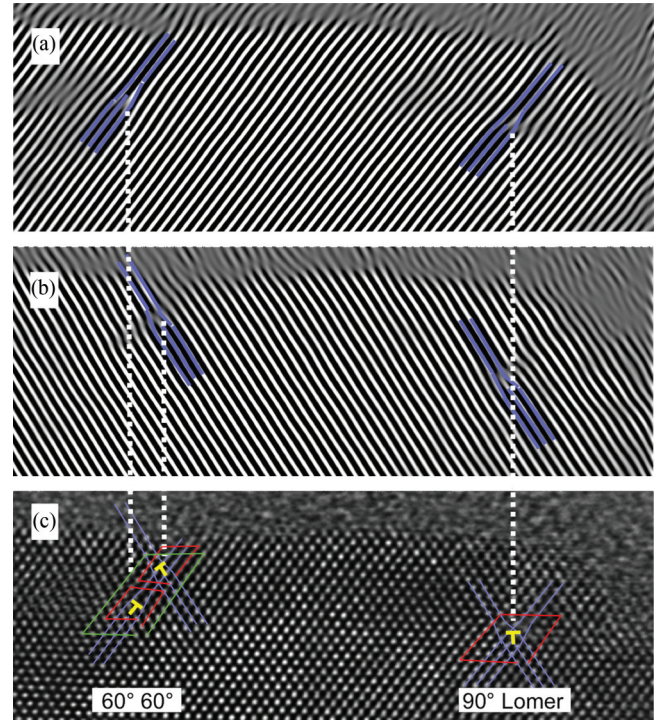


FIG. 1. (Color online) (a) and (b) Inverse HREM-FFT analyses of a defected sample region, focused on specific  $\{111\}$  crystalline planes. (c) Cross-section HREM image of the analyzed sample region. The  $60^\circ$  pair and Lomer dislocation geometries are highlighted, with the relative extra planes (blue online) and Burgers circuits (red online). The larger circuit drawn around the pair (green online) illustrates the correspondence between the relative displacement field and the Lomer one.

HREM analyses were performed through TEM using a JEOL JEM-2010F microscope operated at 200 KeV and equipped with an energy image filter that was tuned up at 0 eV to filter out the background noise introduced by anelastically scattered electrons. HREM images were digitalized and subjected to fast Fourier transform (FFT) processing. The FFT patterns were filtered by selecting specific  $\{111\}$  diffraction spots, and then an inverse FFT process was applied, thus highlighting dislocation positions and characters.

Figure 1 shows an example of HREM-FFT defect analysis [Figs. 1(a) and (b)] and a cross-section HREM image of the considered sample region [Fig. 1(c)]. A Ge depletion region can be observed on the right in Fig. 1(c): the LT used in the deposition does not allow the Ge uniform coverage of the substrate. However, the nominal thickness in the flat film parts is confirmed by TEM and is almost constant ( $3 \pm 0.5$  nm) in the whole sample. Strain was also measured by a FFT analysis of the lattice parameters and gave a residual in-plane strain value of 3.17%. Defects are clearly individuated by the HREM-FFT analysis: a  $60^\circ$  pair and a Lomer dislocation are revealed. The cross-section HREM image in Fig. 1(c) highlights the defect geometries by explicitly reporting the relative Burgers circuits (red in the online version) and the extra planes (blue online). A comparison between the larger circuit (green online) around the close pair and the Burgers circuit around the Lomer dislocation illustrates how,

in few atomic planes, the relative displacement fields become undistinguishable. The close distance between the dislocation cores in the  $60^\circ$  pair turns out to be only 0.9 nm (still not leading to their fusion).

In the sample, 88% of the dislocations found by HREM and analyzed by FFT were clearly coupled (distance  $< 2$  nm) with another dislocation, lying in a mirror symmetric plane; only the remaining 12% were either Lomer dislocations or isolated  $60^\circ$  ones (with similar occurrence). The abundance of  $60^\circ$  pairs, observed in the HREM analysis, demonstrates their major role in the plastic relaxation of the LT-grown thin Ge layer. Although similar pairs have been observed in Ge heterostructures,<sup>9,11,18</sup> their presence has been ascribed to a sort of frustrated Lomer formation process. It has been suggested that the nucleation site of complementary dislocations can statistically lie on different  $\{111\}$  glide planes around the ML plane that should be, in turns, the more favorable nucleation site.<sup>9</sup> On the contrary, we demonstrate in the following that the most probable plane for complementary  $60^\circ$  formation does not correspond to the ML plane and that the  $60^\circ$  pairing follows in the defect evolution as a consequence.

### III. DISLOCATION MODELING

We analytically calculate dislocation-dislocation interactions, as well as their interaction with the epitaxial stress field and with the free surface, in the framework of linear elasticity and dislocation theory.<sup>17</sup> In particular, we investigated the Ge/Si(001) system sketched in Fig. 2, where a straight dislocation ( $\mathbf{b}_1 = a/2[10\bar{1}]$ ) is located along the dislocation line  $\mathbf{l} = [110]$  at the interface. The Ge epilayer thickness ( $h$ ) is equal to 3 nm, as in the CVD deposition.

First, we evaluate along the  $[1\bar{1}0]$  direction the resolved shear stress ( $\sigma_{\text{RSS}}$ ) acting on a second parallel and complementary dislocation ( $\mathbf{b}_2 = a/2[0\bar{1}1]$ ), located  $\sim 1$  nm below the Ge surface<sup>24</sup> to avoid unknown core-related effects due to the close free surface. The  $\sigma_{\text{RSS}}$  values are calculated along the dotted line in Fig. 2(a). The most favored nucleation site for the considered complementary segment (CS) is the position where  $\sigma_{\text{RSS}}$  has the maximum value.

For our system, the  $\sigma_{\text{RSS}}$  value is given by:

$$\sigma_{\text{RSS}} = (\bar{\sigma} \cdot \mathbf{n}_2) \cdot \mathbf{b}_2$$

where  $\mathbf{n}_2 = (1, -1, 1)$  is the normal vector of the CS glide plane, and the stress tensor  $\bar{\sigma}$  is the full stress tensor acting on it, given by

$$\bar{\sigma} = \bar{\sigma}_{\text{het}} + \bar{\sigma}_{\text{surf}} + \bar{\sigma}_{\text{fixed}}$$

where  $\bar{\sigma}_{\text{het}}$  is the biaxial compressive stress due to the lattice mismatch between Ge and Si ( $f = 0.04$ );  $\bar{\sigma}_{\text{fixed}}$  is the exact solution of the stress field generated by the first dislocation at the interface, including the presence of the free surface; and  $\bar{\sigma}_{\text{surf}}$  is the isolated contribution due to the free surface on the second dislocation. In particular, introducing the Ge Young modulus under biaxial stress  $Y$  and defining the  $x$  axis oriented along the  $[1\bar{1}0]$  crystallographic direction, the  $y$  axis along  $[001]$ , and the  $z$  axis along  $[\bar{1}10]$ , the first term in the

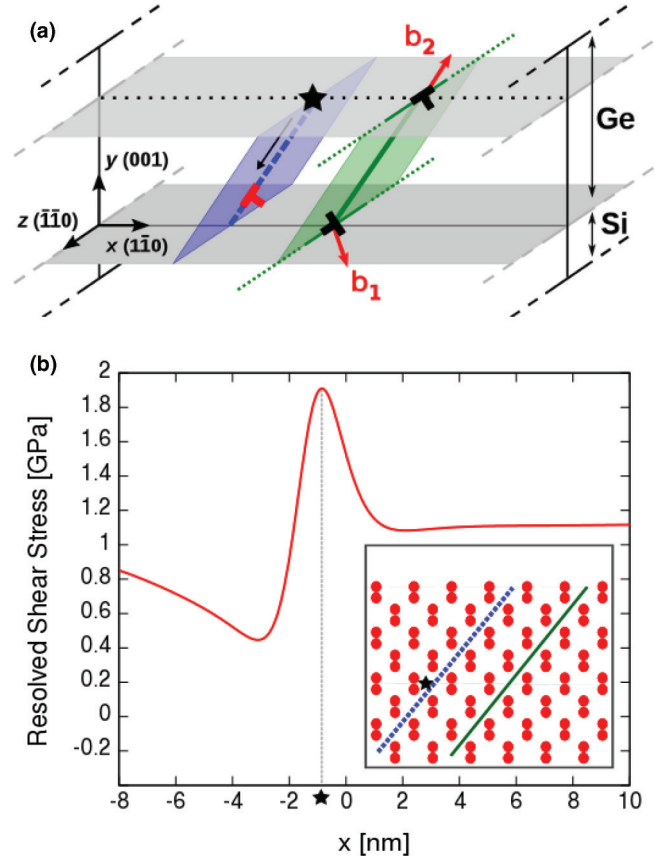


FIG. 2. (Color online) (a) Schematic draw of the configuration analyzed by the analytical model. Burgers vector of the two dislocations are indicated, together with the ML plane (green online; the solid line is drawn as a reference for the printed version and for the graphs in Fig. 3), the  $\sigma_{\text{RSS}}$  maximum position (star), the relative glide plane (blue online; the dashed line is drawn as a reference for the printed version and for the graphs in Fig. 3), and the CS final position (dislocation symbol, red online). (b) Calculated  $\sigma_{\text{RSS}}$  values found along the pointed black line in (a). In the inset, the  $\sigma_{\text{RSS}}$  maximum position (star) is indicated within the crystal, 9 monolayers below the free surfaces.

full stress tensor is simply

$$\bar{\sigma}_{\text{het}} = \begin{pmatrix} -Yf & 0 & 0 \\ 0 & 0 & 0 \\ 0 & 0 & -Yf \end{pmatrix} \quad (1)$$

The  $\bar{\sigma}_{\text{fixed}}$  and  $\bar{\sigma}_{\text{surf}}$  terms, instead, can be computed by using the equations proposed by Head in Ref. 25 for an infinitely long dislocation. We compute separately the contributions in  $\bar{\sigma}_{\text{fixed}}$  due to the three Burgers vector components of the dislocation at the interface, and then we sum the obtained three tensors following the superposition principle.

The screw component  $b_z$  gives rise to the following terms:

$$\sigma_{xz} = \frac{\mu b_z}{2\pi} \left( -\frac{y}{(x^2 + y^2)} + \frac{(y - 2h)}{(x^2 + (y - 2h)^2)} \right) \quad (2)$$

$$\sigma_{yz} = \frac{\mu b_z}{2\pi} \left( \frac{x}{(x^2 + y^2)} - \frac{x}{(x^2 + (y - 2h)^2)} \right) \quad (3)$$



where  $\mu$  is the shear modulus. The free surface contributions (image construction) are represented by the terms explicitly including  $h$  in the preceding equations.

The edge component of the Burgers vector produces two contributions. One arises from the part parallel to the free surface ( $b_x$ ), and the other arises from the part perpendicular to it ( $b_y$ ). In particular  $b_x$  gives

$$\sigma_{xx} = D_x \left( \frac{-y(y^2 + 3x^2)}{(x^2 + y^2)^2} - \frac{(-y + 2h)((-y + 2h)^2 + 3x^2)}{(x^2 + (-y + 2h)^2)^2} - 2h \frac{-y(-y + 2h)^3 - 6(-y + h)(-y + 2h)x^2 + x^4}{((-y + 2h)^2 + x^2)^3} \right) \quad (4)$$

$$\sigma_{yy} = D_x \left( \frac{-y(y^2 - x^2)}{(x^2 + y^2)^2} - \frac{(-y + 2h)((-y + 2h)^2 - x^2)}{(x^2 + (-y + 2h)^2)^2} + 2h \frac{(-3y + 4h)(-y + 2h)^3 - 6(-y + h)(-y + 2h)x^2 - x^4}{((-y + 2h)^2 + x^2)^3} \right) \quad (5)$$

$$\sigma_{xy} = D_x \left( \frac{x(y^2 - x^2)}{(x^2 + y^2)^2} - \frac{x((-y + 2h)^2 - x^2)}{(x^2 + (-y + 2h)^2)^2} + 4h(-y + h)x \frac{3(-y + 2h)^2 - x^2}{((-y + 2h)^2 + x^2)^3} \right) \quad (6)$$

$$\sigma_{zz} = \nu(\sigma_{xx} + \sigma_{yy}) \quad (7)$$

where  $D_x = \frac{\mu b_x}{2\pi(1-\nu)}$  and  $\nu$  is the Poisson ratio.

Instead,  $b_y$  gives

$$\sigma_{xx} = D_y \left( \frac{x(y^2 - x^2)}{(x^2 + y^2)^2} - \frac{x((-y + 2h)^2 - x^2)}{(x^2 + (-y + 2h)^2)^2} + 4hx \frac{(h + y)(-y + 2h)^2 + (-3y + 5h)x^2}{((-y + 2h)^2 + x^2)^3} \right) \quad (8)$$

$$\sigma_{yy} = D_y \left( -\frac{x(3y^2 + x^2)}{(x^2 + y^2)^2} + \frac{x(3(-y + 2h)^2 + x^2)}{(x^2 + (-y + 2h)^2)^2} + 4hx(-y + h) \frac{3((-y + 2h)^2 - x^2)}{((-y + 2h)^2 + x^2)^3} \right) \quad (9)$$

$$\sigma_{xy} = D_y \left( \frac{-y(y^2 - x^2)}{(x^2 + y^2)^2} - \frac{(-y + 2h)((-y + 2h)^2 - x^2)}{(x^2 + (-y + 2h)^2)^2} + 2h \frac{y(-y + 2h)^3 + 6(-y + h)(-y + 2h)x^2 - x^4}{((-y + 2h)^2 + x^2)^3} \right) \quad (10)$$

$$\sigma_{zz} = \nu(\sigma_{xx} + \sigma_{yy}) \quad (11)$$

where  $D_y = \frac{\mu b_y}{2\pi(1-\nu)}$ . All components  $\sigma_{ij}$  ( $i = x, y; j = x, y$ ) are given by the sum of three ratios. The first gives the stress field introduced by an edge dislocation in a bulk system; the second adds the free-surface response, as in the simple image construction; and the third is the correction to the second introduced by Head. Following this consideration,  $\bar{\sigma}_{\text{surf}}$  is obtained exactly as  $\bar{\sigma}_{\text{fixed}}$  (using the CS Burgers vector components and replacing  $h$  with the CS distance from the free surface), but excluding the first addendum in all the  $\sigma_{ij}$  ( $i = x, y; j = x, y$ ) stress-tensor components.

Figure 2(b) presents the obtained  $\sigma_{\text{RSS}}$  values. In the graph, the origin corresponds to the ML plane position ( $x = 0$ ). The maximum  $\sigma_{\text{RSS}}$  site turns out to be off the ML plane. This is shown in the inset, where its position is reported within a Ge crystal lattice (star), together with the relative glide plane (dashed line) and the ML plane (continuous line). This is in agreement with results obtained in a similar system reported in Ref. 19; however, those authors do not model further defect evolution. Here, we have also investigated the migration of the CS along the  $\{111\}$  glide plane from the  $\sigma_{\text{RSS}}$  maximum position toward the heterointerface, where the first segment is kept fixed at its position. In particular, we have evaluated the force acting on CS at different distances  $d$  from the heterointerface.

In the dislocation theory, the force causing the dislocation glide is given by<sup>17</sup>

$$\mathbf{F}_{\text{glide}} = \frac{[(\bar{\sigma} \cdot \mathbf{b}_2) \times \mathbf{l}] \cdot [\mathbf{l} \times (\mathbf{b}_2 \times \mathbf{l})]}{|\mathbf{l} \times (\mathbf{b}_2 \times \mathbf{l})|}$$

The values obtained are reported by the dashed line in Fig. 3 as a function of the normalized distance from the surface  $d/h$ . For comparison, we also analyzed the CS motion when it is supposed to be nucleated in the ML plane, as often assumed in literature (e.g., in Ref. 9). The force values acting on CS in the latter case are presented in Fig. 3 by the continuous line. Positive values drive CS toward the free surface ( $d/h = 0$ ), while negative values drive it toward the interface ( $d/h = 1$ ).

The dynamics described by the two curves are evidently extremely different. Indeed, when the complementary dislocation nucleates at the site where we predict maximum likelihood, it reaches a stable equilibrium position ( $\mathbf{F}_{\text{glide}} = 0$ ) at a distance of  $d/h = 0.8$ , i.e.,  $\sim 7$  Å from the interface, as shown by the dashed line. On the contrary (as reported by the continuous line), we observe that, when the CS nucleates on the ML plane,  $\mathbf{F}_{\text{glide}}$  assumes increasingly negative values, thus accelerating the CS gliding toward the interface where it reaches the first dislocation and where it can react, forming a Lomer dislocation.

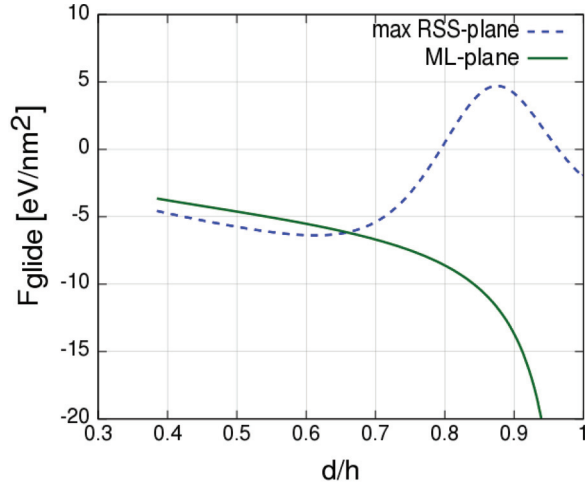


FIG. 3. (Color online)  $F_{\text{glide}}$  values acting on the CS obtained by the analytical model along the ML plane (solid line, green online) and along the glide plane relative to the  $\sigma_{\text{RSS}}$  maximum position (dashed line, blue online).  $d$  is the distance from the interface, and  $h$  is the film thickness.

The main relaxation mechanism founded by the HREM defect analysis, i.e., the dislocation pairing, is fully consistent with the scenario defined by the first dynamics. Therefore, the full form of the stress field ( $\bar{\sigma}$ ), causing the dislocation nucleation and motion, determines both the most favored formation site lying out of the ML plane and the existence of an equilibrium position at a finite distance from the interface. The value of the final dislocation distance from the interface predicted by the continuum model is in good quantitative agreement with that obtained by HREM. At any finite temperature, there also exists a (lower) probability (Fig. 2) to nucleate in the ML plane, not at the maximum  $\sigma_{\text{RSS}}$  position, leading to quick Lomer formation (Fig. 1) according to our model (Fig. 3). A dislocation-position-dependent formulation of all terms composing  $\bar{\sigma}$  has been needed to catch the experimental evidence.

#### IV. MD SIMULATIONS

In order to analyze possible further motion or recombination due to atomic-scale effects, we added to the theoretical investigation a set of dedicated MD simulations.

A simulation cell has been constructed with the  $x$  axis oriented along the  $[1-10]$  crystallographic direction, the  $y$  axis along  $[001]$ , and the  $z$  axis along  $[-1-10]$ , as in the analytical model. Cell sizes are  $59.92 \times 5.4 \times 17.11$  nm, and the total number of atoms is 275 184. Periodic boundary conditions are applied in  $x$  and  $z$  directions. A 3-nm-thick Ge epilayer is located on top of a 14-nm-thick Si substrate. Vacuum is left above the (001) surface, while the bottommost four layers of the Si substrate are kept frozen at their bulk positions.

We introduce in the cell the two dislocation segments considered in the analytical model. The first dislocation is at the interface with Burgers vector  $\mathbf{b}_1 = a/2[10-1]$ , and the complementary one is at the  $\sigma_{\text{RSS}}$  maximum position (star in Fig. 2) with  $\mathbf{b}_1 = a/2[0-11]$ . Both dislocations are inserted using the equations for the displacement field reported in

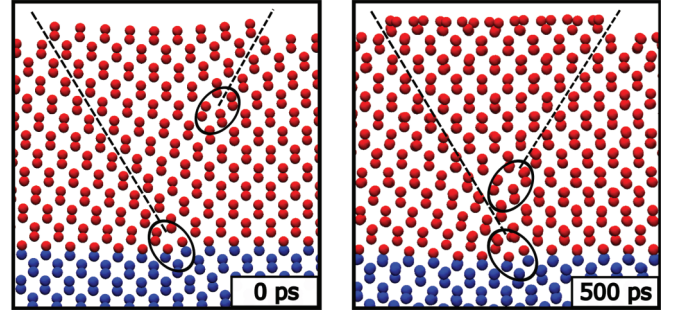


FIG. 4. (Color online) Snapshot of the initial (0 ps) and final (500 ps) configurations in the MD simulation run at 600 K.

Ref. 17. An initial energy minimization is needed in order to settle the core structures and the free surface reaction. Atomic interactions are calculated using the Tersoff potential,<sup>26,27</sup> which has been shown to nicely reproduce typical dislocation behaviors in the present system.<sup>28,29</sup> The total simulation time was set to 500 ps, resolved in steps of 2 fs. Finally, the simulation temperature was set to 600 K to match experiments.

In Fig. 4, we display two close-ups of the simulation cell around the dislocations in the first configuration (CS is in the initial position, determined by the imposed displacement) and the last configuration (CS has migrated to its final position). The CS travels through the layer and then stops above the first at a distance of  $\sim 1$  nm from the interface, reaching the equilibrium position after 290 ps. No further motion has been observed in the residual simulation time. The prediction of the analytical model is thus confirmed, and the experimental evidence is fully reproduced quantitatively by MD. Moreover, as seen in the experiments, MD simulations demonstrate that, for the considered temperatures, core interactions in the closely paired ( $\sim 1$  nm)  $60^\circ$  dislocations do not lead to their fusion, a process that could have escaped from the continuum approach.

Several authors reported on the dominance of Lomer dislocations in LT growth when an increase of the process temperature followed, at some stage, the deposition of the first layers, during either growth or annealing.<sup>3,9,30</sup> Actually, if heating provides sufficient mobility, the  $60^\circ$  dislocation pairs discussed here could possibly lead to the formation of actual Lomer cores. The primary dislocation could leave the interface and glide up to the CS. Alternatively, point defects could be involved, the two dislocations forming a perfect Lomer core via short-range climbing. However, the experimental sensibility required to distinguish a Lomer core from a  $60^\circ$  pair is hardly guaranteed by conventional  $\mathbf{g} \cdot \mathbf{b}$  analyses or Burger circuits. In this respect, further atomically resolved analysis is needed to fully shed light on the processes occurring upon deviating from the LT condition.

#### V. CONCLUSIONS

We have shown that strain relaxation in LT Ge thin films grown on Si(001) proceeds by nucleation of pairs of  $60^\circ$  dislocations, the two cores being close to one another so that a quasi- $90^\circ$  dislocation is created. A continuum model was proposed explaining the observed configuration, also predicting typical dislocation-dislocation distances quantitatively.

Atomic-scale MD simulations also confirmed and reinforced the proposed scenario.

Local thermodynamics seems to determine the positioning of the second dislocation once the first is deposited. This behavior is peculiar of high Ge content

films, activation of heterogeneous nucleation sources (e.g., point defects) becoming instead dominant in the Ge-diluted case. The present results should also be regarded as a starting point for unraveling the more complex HT evolution.

---

\*Corresponding author: [anna.marzegalli@unimib.it](mailto:anna.marzegalli@unimib.it)

<sup>1</sup>J. Stangl, V. Holy, and G. Bauer, *Rev. Mod. Phys.* **76**, 725 (2004).

<sup>2</sup>B. Cunningham, J. O. Chu, and S. Akbar, *Appl. Phys. Lett.* **59**, 3574 (1991).

<sup>3</sup>G. Capellini, M. De Seta, Y. Busby, M. Pea, F. Evangelisti, G. Nicotra, C. Spinella, M. Nardone, and C. Ferrari, *J. Appl. Phys.* **107**, 063504 (2010).

<sup>4</sup>C. Rosenblad, H. R. Deller, A. Dommann, T. Meyer, P. Schroeter, and H. von Känel, *J. Vac. Sci. Technol. A* **16**, 2785 (1998).

<sup>5</sup>R. People and J. C. Bean, *Appl. Phys. Lett.* **47**, 322 (1985).

<sup>6</sup>J. Michel and M. Romagnoli, SPIE Newsroom, doi: [10.1117/2.1201206.004285](https://doi.org/10.1117/2.1201206.004285) (2012).

<sup>7</sup>V. S. Kopp, V. M. Kaganer, G. Capellini, M. De Seta, and P. Zaumseil, *Phys. Rev. B* **85**, 245311 (2012).

<sup>8</sup>W. Hu, B. Cheng, C. Xue, H. Xue, S. Su, A. Bai, L. Luo, Y. Yu, and Q. Wang, *Appl. Phys. Lett.* **95**, 092102 (2009).

<sup>9</sup>Y. B. Bolkhovityanov, A. S. Deryabin, A. K. Gutakovskii, and L. V. Sokolov, *Acta Mater.* **61**, 617 (2013).

<sup>10</sup>E. P. Kvam, D. M. Maher, and C. J. Humphreys, *J. Mater. Res.* **5**, 1900 (1990).

<sup>11</sup>Y. B. Bolkhovityanov and L. V. Sokolov, *Semicond. Sci. Technol.* **27**, 043001 (2012).

<sup>12</sup>R. Hull and J. C. Bean, *J. Vac. Sci. Technol. A* **7**, 2580 (1989).

<sup>13</sup>Y. Chen and J. Washburn, *Phys. Rev. Lett.* **77**, 4046 (1996).

<sup>14</sup>A. Trampert, E. Tournié, and K. H. Ploog, *Appl. Phys. Lett.* **66**, 2265 (1995).

<sup>15</sup>F. K. LeGoues, J. Tersoff, M. C. Reuter, M. Hammar, and R. Tromp, *Appl. Phys. Lett.* **67**, 2317 (1995).

<sup>16</sup>T. J. Gosling, *J. Appl. Phys.* **74**, 5415 (1993).

<sup>17</sup>J. P. Hirth and J. L. Lothe, *Theory of Dislocations* (Krieger, Malabar, FL, 1992).

<sup>18</sup>S. Oktyabrsky, H. Wu, R. D. Vispute, and J. Narayan, *Philos. Mag. A* **71**, 537 (1995).

<sup>19</sup>J. Narayan and S. Oktyabrsky, *J. Appl. Phys.* **92**, 7122 (2002).

<sup>20</sup>Y. Wang, P. Ruterana, S. Kret, J. Chen, S. El Kazzi, L. Desplanque, and X. Wallart, *Appl. Phys. Lett.* **100**, 262110 (2012).

<sup>21</sup>D. J. Smith, *Rep. Prog. Phys.* **60**, 1513 (1997).

<sup>22</sup>D. J. Eaglesham and M. Cerullo, *Appl. Phys. Lett.* **58**, 2276 (1991).

<sup>23</sup>A. Sakai, T. Tatsumi, and K. Aoyama, *Appl. Phys. Lett.* **71**, 3510 (1997).

<sup>24</sup>We use 1.15 nm, because this corresponds to the initial position of the dislocation segment used in the MD simulations discussed later, being compatible with the crystallographic sites.

<sup>25</sup>A. K. Head, *Proc. Phys. Soc. London, Sect. B* **66**, 793 (1953).

<sup>26</sup>J. Tersoff, *Phys. Rev. B* **37**, 6991 (1988).

<sup>27</sup>J. Tersoff, *Phys. Rev. B* **39**, 5566 (1989).

<sup>28</sup>A. Marzegalli, F. Montalenti, and L. Miglio, *Appl. Phys. Lett.* **86**, 041912 (2005).

<sup>29</sup>A. Marzegalli, F. Montalenti, and L. Miglio, *J. Phys. Condens. Matter* **17**, 7505 (2005).

<sup>30</sup>A. Sakai, N. Taoka, O. Nakatsuka, S. Zaima, and Y. Yasuda, *Appl. Phys. Lett.* **86**, 221916 (2005).